Acoustic resonances in HID lamps: model and measurement

John Hirsch, Bernd Baumann, Marcus Wolff, Sounil Bhosle, Ricardo Valdivia Barrientos

Acoustic resonances in HID lamps: Model and Measurement

John Hirsch*[1], Bernd Baumann[2], Marcus Wolff[2], Sounil Bhosle[3,4] and Ricardo Valdivia Barrientos[5]

[1] Lightlabs, Philips Lighting, Eindhoven, the Netherlands
[2] Hamburg University of Applied Sciences, Hamburg, Germany
[3] Université de Toulouse, [4]CNRS; LAPLACE, Toulouse, France
[5] National Institute of Nuclear Research, Salazar, Ocoyoacac, Mexico
* Mathildelaan 1, 5600 JM Eindhoven, The Netherlands, email: john.hirsch@philips.com

Keywords: HID lamp, acoustic resonance, modeling

Abstract. A finite element model including plasma simulation is used to calculate the amplitude of acoustic resonances in HID lamps in a 2D axisymmetric geometry. Simulation results are presented for different operation parameters and are compared with experimental data.

1. Introduction

Today most low power High Intensity Discharge (HID) lamps (20 W to 150 W) used in indoor applications, such as shop lighting, are operated by low frequency square wave (LFSW) drivers. These drivers deliver a square current waveform at a frequency varying from 100 to 400 Hz. A disadvantage of LFSW drivers is that they are relatively bulky. It has been shown [1] that the optimum frequency of operation for the most compact drivers is around 300 kHz. However, at this frequency low power HID lamps suffer from acoustic resonances (AR) which can lead to an unstable plasma arc, causing lamp flicker and sometimes early lamp failure.

Over the past years an enormous effort has been made to investigate and avoid the phenomenon of acoustic resonances in HID lamps. In [2, 3, 4] the frequency dependent fluctuation in light intensity is measured by broadband photodiodes for lamps of different geometries. In [5] lamp geometry and operating frequency schemes are used to reduce the negative effect of acoustic resonances. It is shown that a specific end burner construction in combination with high frequency operation with frequency modulation can indeed reduce instabilities. In [6] another operating method referred to as 'spread spectrum' is also reported to reduce lamp instabilities when operated at high frequency.

Recently more attention has been dedicated to the fundamental understanding and modelling of acoustic resonances. In [7] acoustic streaming is determined as the cause of plasma instabilities in a frequency region where acoustic resonances are excited. Further modelling of acoustic resonances is found in [8] where the Navier-Stokes equation with an imposed standing pressure wave is solved numerically. In [9] the study is extended to the time domain, and the arc motion due to acoustic streaming is calculated. However, there is still a need for an acoustic resonance model which could be used as a fast and convenient tool for the design of HID lamps that are free of AR in given frequency domains. For instance, such a model could be used to determine the effect of the burner pressure and electrode distance on the amplitude of acoustic resonances, and predict the region of stable operation.

In [10] we presented a finite element (FE) model describing the generation of acoustic resonances by an idealized Gauss-shaped excitation. In this article the plasma simulation is added in order to define a realistic temperature and power density profile. In a preprocessing stage, plasma equations are solved in defined gas mixture and burner geometry for a given current. Then, the acoustic modes frequency spectrum is computed using an eigenvalue equation. The amplitude of each mode is finally post-processed. To keep memory and CPU-time requirements reasonable this computing scheme is applied in a 2D axisymmetric geometry. A more realistic treatment would require a 3D model since arc bending violates the axial symmetry.

The model provides the acoustic resonance spectrum of a given lamp. The calculations are performed using the COMSOL Multiphysics Finite Element Method (FEM) tool and the solving time is approximately 30 minutes on a 64 bit computer. Simulation results are presented in this paper for different lamp parameters and are compared with experimental data.

2. Model

2.1 Plasma temperature and power density

The plasma model is used to determine the temperature distribution and power density in the HID burner and these are then used as input for the acoustic calculations. A typical HID lamp is shown in Figure 1 (Philips CDM 70 W). The lamp salt fill consist of a mixture of Sodium, Thallium and Dysprosiym.

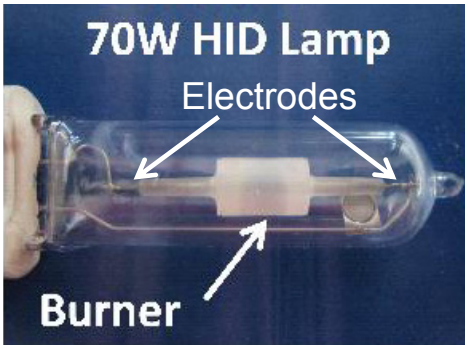

Figure 1. Typical HID lamp (Philips CDM 70 W) used in retail application.

The plasma is considered at Local Thermodynamic Equilibrium (LTE) and no coupling with the electrodes is taken into account. Consequently, the plasma mechanisms are governed by three partial differential equations:

- Current conservation equation for the determination of the distribution of the electric potential.
- Conductive and convective heat transfer equation to determine the local temperature in the plasma.
- Incompressible Navier-Stokes equation to simulate the convection of the burner content.

The first differential equation applies only in the plasma domain:

$$\vec{\nabla} \cdot (-\sigma \vec{\nabla} V) = 0 \qquad (1)$$

It corresponds to current conservation in a conductive medium. V is the electrostatic potential and σ is the electrical conductivity of the gas depending on the pressure and temperature [11].

The boundaries of the plasma domain are set as Neumann boundary conditions:

$$\vec{n} \cdot (-\sigma \vec{\nabla} V) = J_0 . \qquad (2)$$

In this case, J_0 is the inward current density. Its value on the electrode tips is obtained by dividing the applied current by the transversal area of one electrode. This condition ensures a homogeneous current density on the tips. The upper electrode tip is set at a positive value and the lower electrode tip at a negative value. The sides of the electrodes and the walls of the lamp are defined as insulation condition ($J_0 = 0$). The initial value of the potential is set to $V(t_0) = 0$.

The temperature distribution inside the burner is obtained from

$$\vec{\nabla} \cdot (-\kappa \vec{\nabla} T) = Q - \rho C_p \vec{U} \cdot \vec{\nabla} T \tag{3}$$

(κ thermal conductivity [11], T temperature, ρ mass density, $\vec{U}$ vector of velocity, C_p heat capacity at constant pressure, Q heat source density).

The source term is calculated from

$$Q = \sigma E^2 - q, \tag{4}$$

with the electrical field $E = \left| -\vec{\nabla} V \right|$. The temperature dependent quantity q is defined by an interpolation function and introduced to account for radiation losses [12, 13]. The mass density is calculated from the ideal gas law

$$\rho = \frac{pM}{RT} \tag{5}$$

(p static pressure of the gas, M molar mass of the gas = 0.2 kg mol^{-1} for Hg, R = 8.32 J K^{-1}mol^{-1} the perfect gas constant).

Equation (3) is applied to the three domains (plasma, electrodes and walls). For the electrodes the coefficients κ, ρ and C_p are used directly from the library of the material "aluminum" in the COMSOL material database, the vector $\vec{U}$ is set at $\vec{0}$ in the electrode domain as there is no convection, and the coefficient Q is also set as 0.

For the wall of the burner, κ, ρ and C_p are set according to the values of the polycrystalline alumina (PCA) as 12 W m^{-1}K^{-1} [14], 2203 kg m^{-3}, and 703 J kg^{-1}K^{-1}, respectively. The vector $\vec{U}$ is set as $\vec{0}$ and Q is also set as 0.

Finally, for the gas Hg, the coefficient κ is set as an interpolation function depending on the temperature [11], ρ is according to Equation (5), C_p is considered constant as 114 J kg^{-1}K^{-1}, the components of the vector $\vec{U}$ are calculated from the Navier-Stokes Equation (8), and the term Q is set according to Equation (4).

The boundaries conditions are set as follows: For the external edges of the electrodes, temperature boundary conditions are used with a constant value of T_0 = 500 K. This temperature corresponds to an evaluation of the temperature when the lamp is in steady state. However, this value has a weak influence on the plasma temperature profile and a precise value is therefore not required.

In a lamp, the burner is usually placed under vacuum in an outer glass bulb. It is consequently not affected by conduction and convection with an outer gas. Thus, it is assumed to lose its thermal energy by radiation only. As a result, for the external faces of the walls of the burner, the heat flux is specified according to:

$$\vec{n} \cdot \kappa \vec{\nabla} T = q_0, \tag{6}$$

where the inward heat flux q_0 is calculated from the Stefan-Boltzmann law

$$q_0 = -\sigma T^4 \tag{7}$$

with the Stefan-Boltzmann constant $\sigma = 5.6704\text{x}10^{-8}$ $\text{Wm}^{-2}\text{K}^{-4}$ and the emissivity assumed to be 1.

The initial temperature $T(t_0)$ should not affect the final solution of the temperature profile. However, considering the nonlinearity of the equation system, an initial temperature profile close to the steady state solution is required. This prevents unrealistic solutions or long computing time. Consequently, $T(t_0)$ is defined according an interpolation function implemented from the experimental temperature profile measured on a 70W CMH lamp. Figure 2 displays the temperature profile for a unit radius.

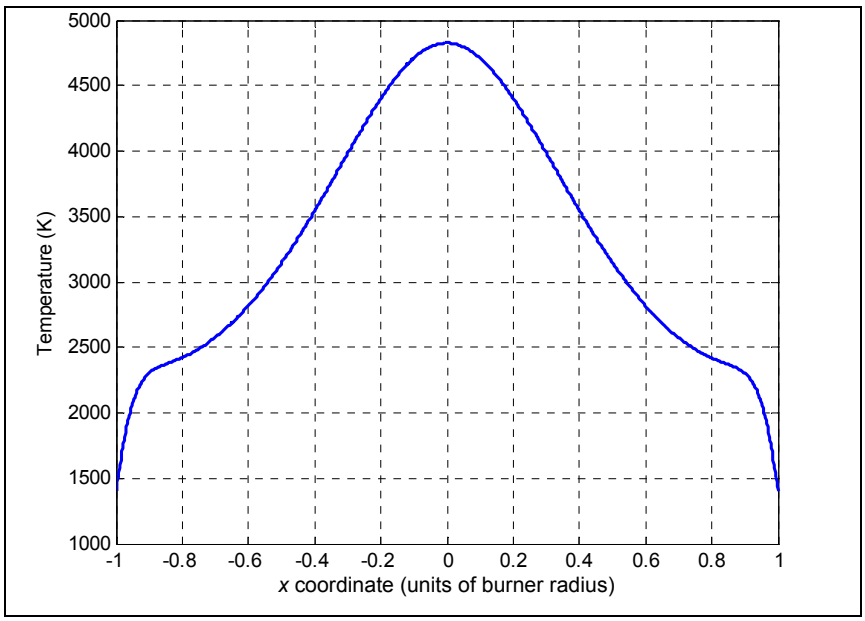

Figure 2. Initial temperature profile chosen for the modeling based on a Philips CDM 70W measurement using X-ray photo-absorption.

The incompressible Navier-Stokes is solved to compute the velocity field of the fluid

$$\rho\left(\vec{U}\cdot\vec{\nabla}\right)\vec{U} = \vec{\nabla}\cdot\left[-p\vec{I} + \eta\left(\vec{\nabla}\vec{U} + \left(\vec{\nabla}\vec{U}\right)^{T}\right)\right] + \vec{F} \qquad (8)$$

(η viscosity of the fluid, $\vec{F}$ volume force, $\vec{I}$ identity operator).

Equation (8) is applied only to the domain corresponding to the plasma. The coefficient η is set as an interpolation function depending on the temperature [11], ρ is set according to Equation (5). The vertical component of the volume force $\vec{F}$ is set to -10ρ (gravity force). As boundary conditions $\vec{U} = \vec{0}$ (no slip) is used.

It is important to establish one point constraint for the pressure on the interior boundary. In this case, the point is placed at the vertices formed by the union of the lower electrode with the internal edge of the wall. The value of this point is set at the static pressure chosen for the lamp.

The initial value for the Equation (8) is $\vec{U}(t_0) = \vec{0}$, and $p(t_0)$ is set at the static pressure of the lamp.

The plasma modeling described in this paragraph is quite simple and approximate. Considering the plasma at LTE, without any sheath, does not describe the fine mechanisms involved in this arc discharge plasma. However, it provides a satisfactory temperature profile in a relatively short computing time and with reasonable memory requirement for a desktop computer. This temperature profile is then used as the input parameter for the computing of the acoustic modes.

2.2 Acoustic pressure

As a result of the alternating current the lamp filling is periodically heated. Therefore, an acoustic wave with the modulation frequency of the power is generated. It propagates towards the walls where it is damped and reflected. Incident and reflected waves interfere which leads to the development of standing acoustic waves. At certain frequencies resonances form. The standing waves interact with the discharge arc and are responsible for its distortion and instability. In this section the calculation method of the acoustic amplitudes is described. Details can be found elsewhere [15, 16].

The starting point is the inhomogeneous Helmholtz equation for the acoustic pressure [17, 18]:

$$\vec{\nabla}\left(\frac{1}{\rho}\vec{\nabla}p\right)+\frac{\omega^2}{\rho c^2}p=i\omega\frac{\gamma-1}{\rho c^2}H \tag{9}$$

where γ denotes adiabatic index. $H(\vec{r},\omega)$ constitutes the Fourier transform of the power density deposited in the gas as computed from $\sigma \cdot E^2$.

The temperature T in the burner is not uniform but space dependent. The density ρ of the burner filling and the speed of sound c attain a space dependency as well. In this work, it is assumed that the relation of T and ρ is described by the ideal gas law Equation (5), and c and T are related through $c=\sqrt{\gamma R_m T/M}$.

Loss is accounted for via loss factors. The surface loss factor associated to the *j*-th acoustical eigenmode with p_j eigenfrequency ω_j of the burner (volume V_B) resulting from shear stress is calculated from the surface integral

$$L_j^{(s_\eta)}=\frac{1}{\sqrt{2\omega_j}\omega_j^2 V_B}\int_{S_B}\sqrt{\frac{\eta}{\rho}}c^2\left|\vec{\nabla}_t p_j\right|^2 dS \tag{10}$$

$\vec{\nabla}_t p_j$ denotes the component of the pressure gradient tangential to the burner wall and the integral has to be taken over the entire surface of the burner. Surface loss due to heat conduction can be calculated from the similar integral

$$L_j^{(s_\kappa)}=\frac{\gamma-1}{\sqrt{2C_p\omega_j}V_B}\int_{S_B}\sqrt{\frac{\kappa}{\rho}}\left|p_j\right|^2 dS\,. \tag{11}$$

The integrals contain the associated transport coefficients η (coefficient of viscosity) and κ (coefficient of heat conduction) respectively.

Equation (11) is derived under the assumption that the thermal conductivity of the wall is very large compared to the thermal conductivity of the gas. A rough estimation of the ratio of the thermal conductivities results in $\kappa_{\text{wall}}/\kappa_{\text{plasma}}=O(50)$. This is considered to be large and justifies the use of Equation (11).

Volume loss due to shear stress is described by:

$$L_j^{(v_\eta)}=\frac{4}{3\rho c^2}\sum_i\omega_i\left(\frac{A_i}{A_j}\right)^*\frac{1}{V_B}\int_{V_B}\eta p_i^* p_j dV\,. \tag{12}$$

This equation is derived by following the reasoning in [19, 20] and considering $\rho c^2 = \text{const}$. The amplitudes A_i and A_j are defined below. If η were constant, the above sum is reduced to a single term due to the orthogonality of the normalized eigenmodes p_j.

In order to allow an estimation of the loss factor (see Equation (12)), we describe the viscosity as the sum of a constant and a space dependent part:

$$\eta(\vec{r}) = \overline{\eta} + \hat{\eta}(\vec{r}). \tag{13}$$

$\overline{\eta}$ is chosen to be the mean value between the largest and smallest viscosity inside the burner. This leads to

$$L_j^{(v_\eta)} = \frac{4\overline{\eta}}{3\rho c^2}\omega_j + \text{corrections}. \tag{14}$$

For volume loss due to thermal conduction we proceed in the same way. Splitting the coefficient of thermal conduction

$$\kappa(\vec{r}) = \overline{\kappa} + \kappa(\vec{r}) \tag{15}$$

leads to

$$L_j^{(v_\kappa)} = \frac{(\gamma-1)\overline{\kappa}}{C_p \rho c^2}\omega_j + \text{corrections}. \tag{16}$$

In order to check if the correction terms in Equations (14) and (16) are negligible, we make the following estimation: Ignoring these corrections and using reasonable values for the physical quantities one can calculate the two volume loss factors. In this approximation volume loss scales linearly with frequency:

$$L_j^{(v)} = L_j^{(v_\eta)} + L_j^{(v_\kappa)} \propto \omega_j. \tag{17}$$

Critical damping corresponds to $L_j^{(v)} = 2$ and, therefore, occurs at a frequency $f_{\text{crit}} \approx 1\,\text{GHz}$. It is very unlikely that the correction terms would change f_{crit} by orders of magnitude, and it is reasonable to disregard the corrections in the volume loss formulas for the frequency range considered in this paper [10].

The solution of the Helmholtz equation can be expressed as a superposition of the normalized eigenmodes

$$p(\vec{r},\omega) = \sum_j A_j(\omega) p_j(\vec{r}), \tag{18}$$

where the contribution of a certain mode is determined by the frequency dependent amplitudes $A_j(\omega)$. These amplitudes exhibit a Lorentzian profile according to

$$A_j(\omega) = \mathrm{i}\frac{\mathrm{A}_j\omega}{\omega^2 - \omega_j^2 + \mathrm{i}\omega\omega_j L_j}. \tag{19}$$

The excitation amplitude A_j corresponding to the j-th mode is calculated from a scalar product of the mode and the power density profile

$$\mathrm{A}_j = \frac{(\gamma - 1)}{V_B} \int_{V_B} p_j^* H dV \,. \tag{20}$$

3. Experiment

The HID lamp is operated with modulated current. A function generator (Agilent 33220A) is used to define wave shape and frequency. The signal from the function generator is amplified by a high frequency amplifier (Amplifier Research 800A3) and fed to the lamp.

The amplitude of the acoustic resonances is not directly detectable, i.e. we are not able to measure pressure level and fluctuations inside of the burner. However, acoustic resonances can have visible effects on the plasma arc. Three main instability modes can be observed:

- Plasma arc bending
- Plasma arc rotation
- Plasma distortion resulting in light output fluctuation (light flicker)

We measure these effects by monitoring the electrical parameters of the lamp using a power analyzer and the light fluctuation with a photodiode:

- The lamp voltage gives an indication on arc bending, if an increase is measured, or arc straightening, if a decrease is measured.
- The lamp voltage deviation indicates arc rotation or other arc instabilities. The deviation is calculated using 5 consecutive voltage measurements and comparing them to a reference voltage.
- Light flickering indicates arc distortions.

For the measurements the lamp is initially operated at a high reference frequency of 1.2 MHz where no instabilities are observed. At this frequency the reference voltage and current are measured.

In order to determine the flicker level the lamp's emission is collected using an optical fiber and measured with a photodiode (UDT PIN_10AP). After that, the DC part s_{DC} and the AC part s_{AC} (peak-to-peak) are separated. A fast Fourier transform is applied to the AC signal so as to identify the different frequency components. For a specific frequency f_1, the flicker level is defined as

$$F(f_1) = \frac{s_{\mathrm{AC}}(f_1)}{s_{\mathrm{DC}}} \times 100\% \tag{21}$$

The frequency is then decreased in fixed increments of 1 kHz from 1.2 MHz to a frequency where the recorded instabilities became too intense. The time between two successive frequency steps is set at 60 s. After 10 successive measurements, the operating frequency returned to the reference where electrical parameters as well as light flicker are measured again. A schematic of the experimental set-up is shown in Figure 3.

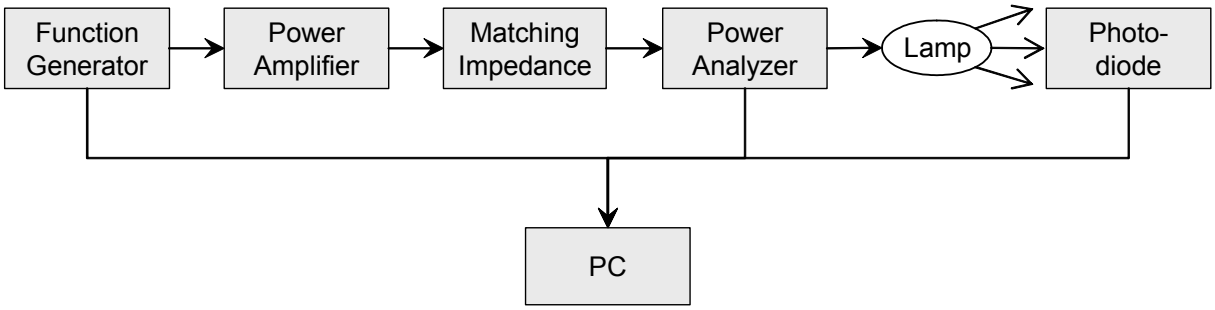

Figure 3. Schematic experimental set-up.

4. Results

We investigated an HID lamp with a somewhat unconventional burner shape that was especially designed and manufactured for this investigation. The burner is made of PCA. A cut through its rugby-shape geometry and the different domains are shown in Figure 4 (right half only). The investigated lamp featured an electrode distance of 5 mm and an inside pressure of $15 \cdot 10^5$ Pa and a salt mixture filling consisting of Sodium, Thallium, Dysprosium. It was operated in vertical position at a voltage around 60 V (power: 20 W).

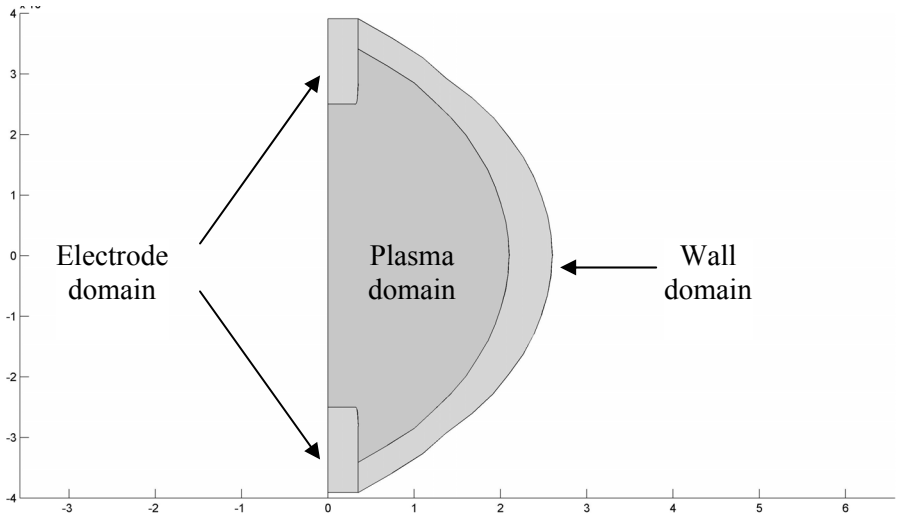

Figure 4. Geometry and different domains of the HID lamp (dimensions in mm).

Two different modulation techniques were applied to the HID lamp and in the following subsections theoretically and experimentally investigated:

- Modulation with constant frequency (subsection 4.1).
- Frequency modulation with 10 kHz around the center frequency (subsection 4.2).

We measured the lamp's voltage fluctuation and flicker level as a function of frequency using the experimental set-up and procedure described in section 3. Then we calculated the amplitudes of acoustic resonances using Equation (18).

Since the response function considerably depends on the location for which it is determined, we calculated it for two different locations inside the burner:

- Center of burner between the electrodes.
- Center of the burner but at the wall.

In the following subsections all frequencies refer to power frequencies.

4.1 Modulation with constant frequency

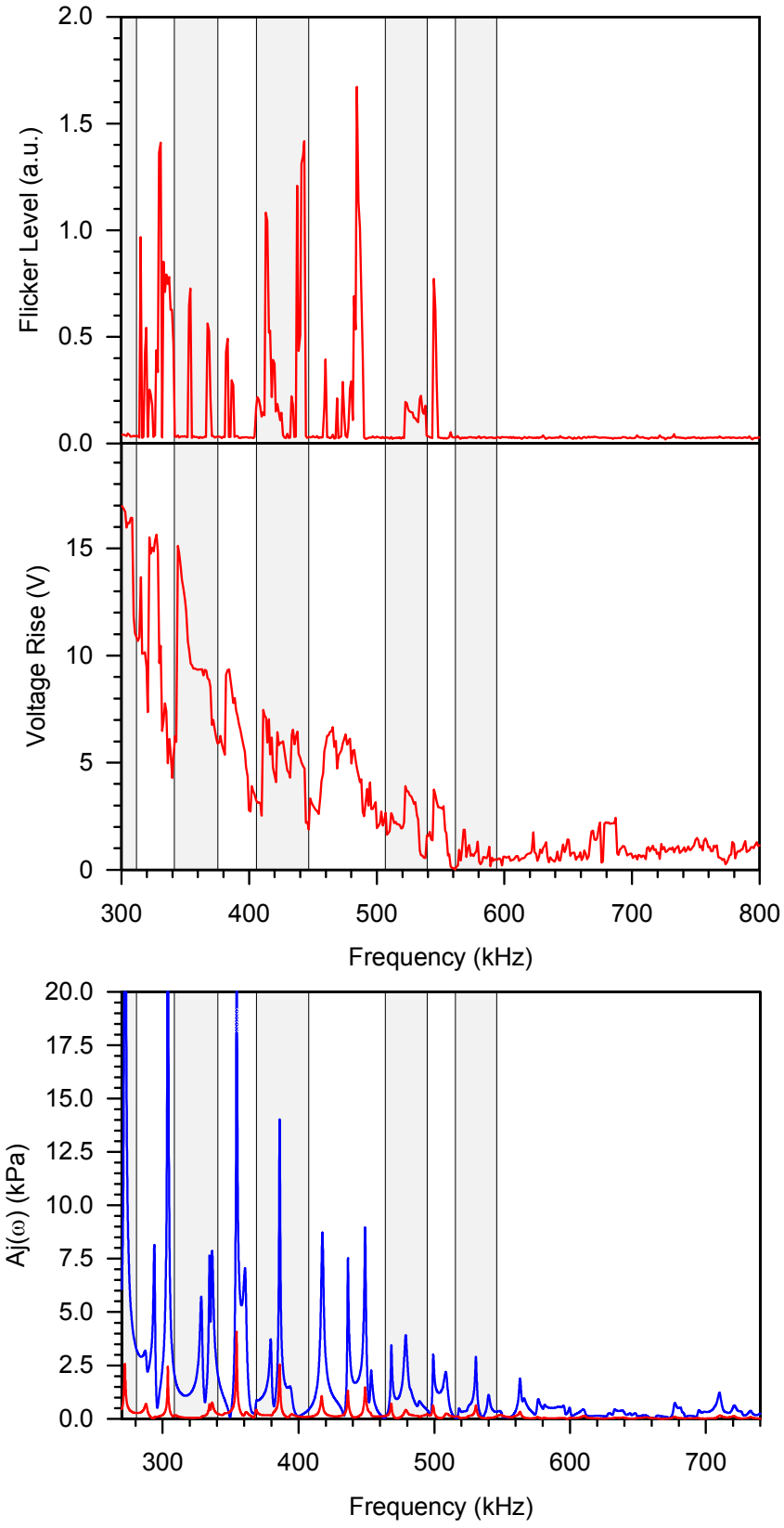

Figure 5. Results for the HID lamp operated at a modulation with constant frequency. Top: Light flicker level measurement. Middle: Lamp voltage measurement. Bottom: Calculated acoustic resonance amplitudes (blue curve is pressure in the center of burner; red curve is pressure in the vertical center of the burner but at the wall).

The two upper graphs of Figure 5 show the results of the measurements for the HID lamp operated at a modulation with constant frequency between 300 and 800 kHz. The flicker level can be seen in the top and the voltage rise in the middle diagram. Below 300 kHz instabilities became too intense and the experiment had to be aborted. The bottom graph displays the acoustic resonance amplitudes that have been calculated using Equation (18) in the frequency range 270 to 740 kHz. The blue curve represents the pressure in the center of burner. The red curve represents the pressure in the vertical center of the burner but at the wall.

The resulting features in the three graphs have been distinguished in terms of color in order to simplify the correlation. It can be seen clearly that the two measurements and the calculation are in good agreement. Every single peak of the voltage measurement can be found in the simulation as well. Due to the increased width of the measured peaks they appear merged. The discrimination for the calculation is considerably more distinct. The resonance frequencies according to the simulation are 20-40 kHz (approximately 7 %) shifted to lower frequencies compared to the measured values.

The features of the flicker level measurement are similar pronounced as the simulation. However, not all of the peaks of the voltage measurement and calculation can be found. The weaker ones are missing. Comparing voltage and flicker level curves it can be concluded, that resonances corresponding to a voltage rise of 3 V and larger are detectable as light flicker. Therefore, the voltage rise is the more sensitive indicator for arc instabilities than the flicker level.

4.2 Frequency modulation

Due to extraordinary intense instabilities it is not possible to modulate the HID lamp with constant frequency below 300 kHz. Applying a frequency modulation instead influences directly the power density H by spreading the power over a wide frequency range. This reduces the energy deposition per frequency unit and, therefore, the excitation of acoustic resonances. Thus, a frequency modulation should bring the weaker acoustic resonances below a critical pressure value, leaving only the strong resonance to be measurable.

Figure 6 shows the results for the HID lamp operated at a 10 kHz frequency modulation between 200 kHz and 400 kHz. The flicker level measurement can be seen in the top diagram. A voltage rise was not recorded for this constellation. The bottom graph displays the acoustic resonance amplitudes in the frequency range from 180 to 400 kHz. Again, the blue curve represents the pressure in the center of burner and the red curve the pressure in the vertical center of the burner but at the wall.

The resulting features have been distinguished in terms of color. Measurement and calculation clearly are in good agreement. Every peak of the flicker level measurement can be found in the simulation as well. Again, the measured peaks are wider than those of the calculation and shifted approximately 20-40 kHz. The relative heights of the peaks are also in reasonable agreement.

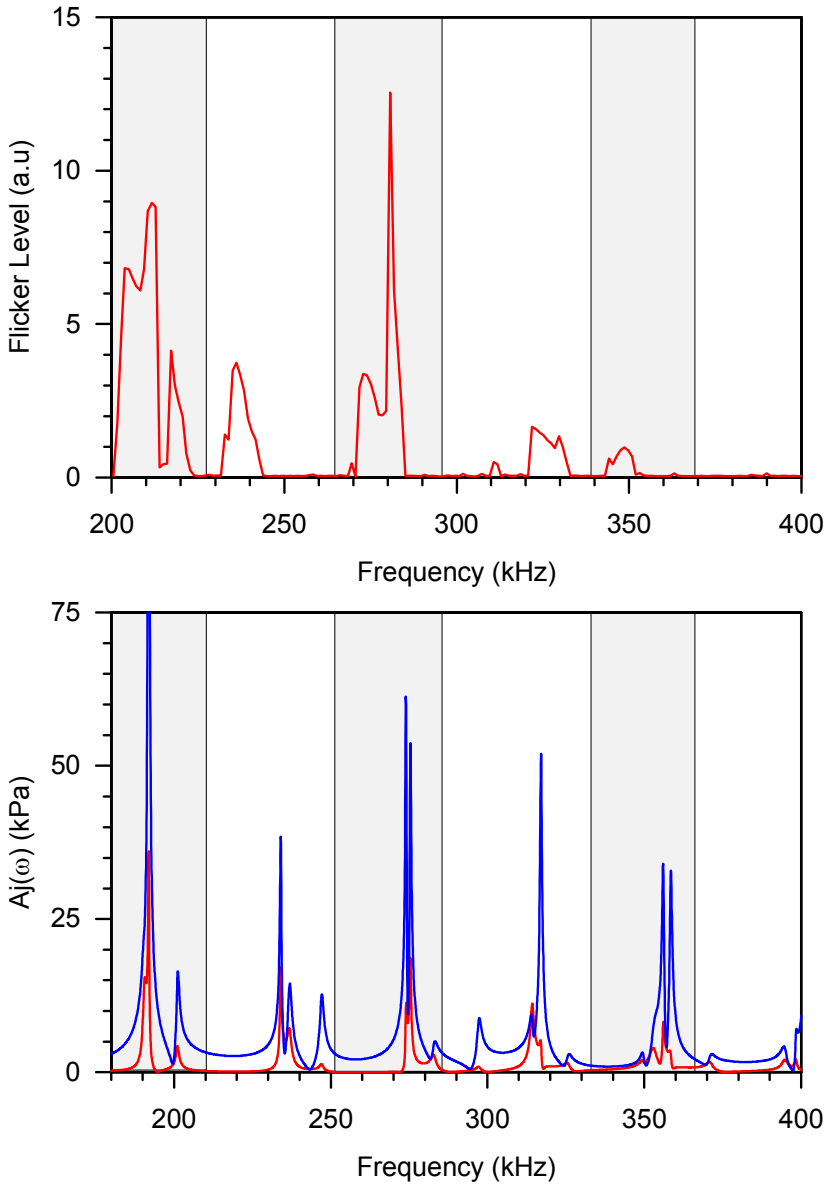

Figure 6. Results for the HID lamp operated at frequency modulation. Top: Light flicker level measurement. Bottom: Calculated acoustic resonance amplitudes. Blue curve is pressure in the center of burner; red curve is pressure in the vertical center of the burner but at the wall.

5. Conclusion

The amplitudes of acoustic resonance in HID lamps have been calculated using FE method. The model includes the calculation of plasma behavior and acoustic pressure amplitudes. Simulation results have been compared to measurements on a prototype 20 W HID lamp that has been operated at two different modulation techniques. For modulation at constant frequency as well as for frequency modulation measurement and calculation were found to be in good agreement concerning resonance frequency and relative amplitude height. The explanation for the small frequency shift between calculation and measurement is probably a slight deviation in the model's gas parameters from the actual values. The relative heights of the peaks are in reasonable agreement as well.

This publication presents first results. Although preliminary they proof the potential of the model as a powerful tool for lamp design. More cases and different burner geometries need to be investigated in order to obtain a reliable model/experiment calibration. This is ongoing work. The model still holds certain limitations. Its 2-dimensionality assumes rotational symmetry. Therefore, arc bending and the like cannot be simulated. The goal is to further develop the model to a stage that allows predicting

frequency regions of stable operation for any given burner shape and set of operation parameters and enabling the use of compact driver electronics.

References

[1] G. Trestman, Minimizing Cost of HID Lamp Electronic Ballast. 28th Annual Conference of the Industrial Electronics Society, IEEE 2002 p 1214-1218.

[2] J. Olsen, W.P. Moskowitz, Optical Measurement of Acoustic Resonance Frequencies in HID lamps, IEEE IAS annual meeting 1997.

[3] J. Olsen, W.P. Moskowitz, Time Resolved Measurements of HID Lamp Acoustic Frequency Spectra, IEEE IAS annual meeting 1998.

[4] J.C. Anton, C. Blanco, F. Ferrero, J. Viera, N. Bordel, G. Zissis, Acoustic Resonance Band detection Workbench for HID lamps, IEEE conference 2004.

[5] S. Wada, A. Okada, S. Morii, Study of HID lamps with reduced Acoustic Resonances, Journal of the Illuminating Engineering Society, 1987.

[6] R. van Honschooten, Philips Power Conversion Symposium, 2007.

[7] F. Afshar. The Theory of Acoustic Resonance and Acoustic Instability in HID lamps. LEUKOS, 20(1):27–38, 2008.

[8] Z. Araoud, S. Kaziz, M. Ben Haj Rhouma, K. Charrada, G. Zissis and M. Sassi. Resolution of Navier-Stokes equations in an acoustic resonance condition of a high pressure mercury lamp. In G. Zissis, editor, Light sources 2004: Proceedings of the 10th International Symposium on the Science and Technology of Light Sources, pages 207–208, Bristol, 2004. Institute of Physics Publishing.

[9] Th.D. Dreeben. Modeling of fluid mechanical arc instability in pure-mercury HID lamps. J. Phys. D: Appl. Phys. 41:144023, 2008.

[10] B. Baumann, M. Wolff, J. Hirsch, P. Antonis, S. Bhosle, R. V. Barrientos, Finite element estimation of acoustical response functions in HID lamps, J. Phys. D. 42 (2009) 225209

[11] P. Flesch, HID lamps, Habilitationsschrift, Universität Karlsruhe (TH), January 2006.

[12] J.J. De Groot., J.A. Van Vliet: The high pressure sodium lamp (Philips Technical Library, 1986)

[13] CLUB EDF ARC ÉLECTRIQUE: L'arc électrique et ses applications (Tome 1, Étude physique de l'arc électrique, Édit. CNRS, 1984)

[14] G.C. Wei, Transparent ceramic lamp envelope materials, J. Phys. D: Appl. Phys. 38, 2005.

[15] B. Baumann, M. Wolff, B. Kost, H. Groninga. Solving a coupled field problem by eigenmode expansion and finite element method. International Journal of Multiphysics, 1(3):303–315, 2007.

[16] B. Baumann, B. Kost, M. Wolff, H. Groninga. Modeling and numerical investigation of photoacoustic resonators. In G. Petrone and G. Cammarata (Ed.), editors, Recent Advances in Modelling and Simulation, pages 17 – 38, Vienna/Austria, 2008. I-Tech Education and Publishing.

[17] B. Baumann, B. Kost, H. Groninga and M. Wolff. Eigenmode Analysis of Photoacoustic Sensors via Finite Element Method. Rev. Sci. Instrum., 77, 044901, 2006.

[18] B. Baumann, M. Wolff, B. Kost, and H. Groninga. Finite element calculation of photoacoustic signals. Applied Optics 46:1120–1125, 2007.

[19] P.M. Morse and K.U. Ingard. Theoretical Acoustics. Princeton University Press, 1987.

[20] L.B. Kreuzer. The physics of signal generation and detection. In Y.-H. Pao, editor, Optoacoustic Spectroscopy and Detection, pages 1–25, London, 1977. Academic.